Spectroscopic and Molecular Docking Study of the Interaction between Neutral Re(I) Tetrazolate Complexes and Bovine Serum Albumin

Spectroscopic and Molecular Docking Study of the Interaction between Neutral Re(I) Tetrazolate Complexes and Bovine Serum Albumin

Joanna Lazniewska,[a] Mark Agostino,[b] Shane M. Hickey,[a] Emma Parkinson-Lawrence,[a] Stefano Stagni,[c] Massimiliano Massi,*[d] Douglas A. Brooks,[a] and Sally E. Plush*[a]

Abstract: Re(I) complexes have potential in biomedical sciences as imaging agents, diagnostics and therapeutics. Thus, it is crucial to understand how Re(I) complexes interact with carrier proteins, like serum albumins. Here, two neutral Re(I) complexes were used (*fac*-[$Re(CO)_3$(1,10-phenanthroline) L], in which L is either 4-cyanophenyltetrazolate **(1)** or 4-methoxycarbonylphenyltetrazole ester **(2)**, to study the interactions with bovine serum albumin (BSA). Spectroscopic measurements, calculations of thermodynamic and Förster resonance energy transfer parameters, as well as molecular modelling were performed to study differential binding between BSA and complex **1** and **2**. Induced-fit docking combined with quantum-polarised ligand docking were employed in what is believed to be a first for a Re(I) complex as a ligand for BSA. Our findings provide a basis for other molecular interaction studies and suggest that subtle functional group alterations at the terminal region of the Re(I) complex have a significant impact on the ability of this class of compounds to interact with BSA; which is important for the functional design of Re(I) complexes in biomedical applications.

Introduction

Re(I) complexes have shown promise in the life sciences due to their unique physicochemical properties, with applications in cellular imaging, diagnostics and as therapeutics. Re(I) complexes have multiple advantages over organic fluorophores for cellular applications, including long exited state lifetimes, large Stoke shifts and high photostability.[1,2] Moreover, Re(I) complexes can be engineered to exhibit low cytotoxicity, which enables live cell imaging applications.[3–5] Indeed, Re(I) complexes have been successfully employed to visualise different cellular structures in cells and tissues including lipid droplets,[4,6] endoplasmic reticulum,[3] mitochondria,[7] autophagosomes,[4] plasma membrane,[3] endosomes,[7] nucleus and the nucleolus,[7] as well as to stain cell membranes/cell walls in bacteria,[8] yeasts[8] and plants.[9] We have focused on the development of neutral Re(I) complexes of the type *fac*-[$Re(CO)_3$(phen)L], where phen = 1,10-phenanthroline and L represents a substituted tetrazolate anion (e. g. 4-cyanophenyltetrazolate) as ancillary ligand. While the tetrazole group offers key advantages, such as the conferral of reduced cytotoxicity, we have shown that different cellular uptake and localisation patterns can be achieved by subtle changes in functional moieties tethered to the tetrazolate ancillary ligand.[2] The ability to modify the Re(I) complex structure adds to the functional potential, which has already been evaluated for diagnostic imaging/radiotherapy,[10] as probes for amyloid fibrils,[11] and enhancers of anticancer drugs.[12] A critical example of how Re(I) complexes have demonstrated diagnostic potential is our work with ReZolve-L1™, which accumulates in prostate cancer cell lines to a much larger extent than in normal prostate cells.[13] The quest to design complexes for cellular and in vivo applications is ongoing and it is therefore important to understand the molecular interactions that contribute to the functionality of these complexes.

One of the most abundant proteins in blood are serum albumins, which have important physiological roles, including acting as carriers for fatty acids, steroids and hormones.[14,15] Interestingly, albumins are also used as carrier proteins for increased drug uptake.[16] For the in vitro and in vivo use of Re(I) compounds to be realised, we need to understand how they interact with albumins as this interaction will influence uptake,

[a] *Dr. J. Lazniewska, Dr. S. M. Hickey, Dr. E. Parkinson-Lawrence, Dr. D. A. Brooks, Dr. S. E. Plush*
Clinical and Health Sciences
University of South Australia
North Terrace, Adelaide SA 5000 (Australia)
E-mail: sally.plush@unisa.edu.au

[b] *Dr. M. Agostino*
Curtin Health Innovation Research Institute
Curtin Institute for Computation and Curtin Medical School
Curtin University
Kent Street, Perth WA 6102 (Australia)

[c] *Dr. S. Stagni*
Department of Industrial Chemistry ''Toso Montanari''
University of Bologna
Viale del Risorgimento 4, Bologna (Italy)

[d] *Dr. M. Massi*
Department of Chemistry
Curtin University
Kent Street, Perth WA 6102 (Australia)
E-mail: M.Massi@curtin.edu.au

distribution, stability, absorption and turnover. Bovine serum albumin (BSA) is commonly used in cell culture systems and is also often used as a model system for human in vivo interactions, due to its sequence homology with human serum albumin (HSA); ~76% homology.[17,18]

Based on our interest in exploring the potential for neutral Re(I) complexes for imaging and as in vivo diagnostics, we report here the structural investigation of two Re(I) *fac*-[Re(CO)$_3$(phen)L] complexes where L = 4-cyanophenyltetrazolate **1** (also referred to as ReZolve-L1^{TM}) and 4-methoxycarbonylphenyltetrazole ester **2** (Figure 1) with BSA. To examine the interactions between the Re(I) compounds and BSA, we used spectroscopic methods and employed molecular modelling to investigate how Re(I) complexes interact as binding partners for BSA. Thus, our work provides a useful tool that can be applied for molecular docking studies of similar ligands and an insight into how the different functional group of the Re(I) complexes **1** and **2** (nitrile and methyl ester, respectively) alter the binding with BSA. This type of investigation will be critical for the design of Re(I) complexes to be exploited as molecular probes.

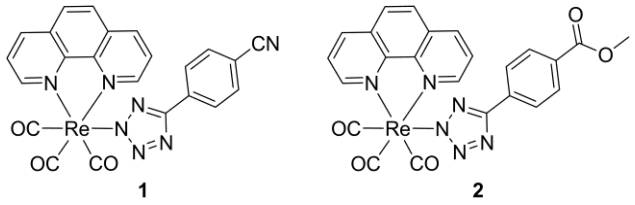

Figure 1. Structures of Re(I) complexes **1** and **2**.

Results and Discussion

The effect of adding variable amounts of Re(I) complexes on BSA absorption and emission spectra

Complexes **1** and **2** were employed for this study to assess their different binding properties with BSA. The preparation and photophysical properties of complexes **1** and **2** have been previously reported.[19,20] BSA is intrinsically fluorescent due to its two tryptophan, 20 tyrosine and 27 phenylalanine residues.[21] The emission from BSA is mainly attributed to Trp134 (found on the surface of subdomain IB) and Trp213 (located within a hydrophobic pocked of subdomain IIA), due to the high molar absorptivity of tryptophan.[22] BSA has several well documented binding sites; the most important of which are sites I and II, which are located in hydrophobic cavities of subdomains IIA and IIIA, respectively.[14,15] When BSA interacts with small molecules, the environment of its fluorescent amino acids is altered, which results in measurable changes in BSA's absorption and emission profiles.

Small molecules alter the emissive properties by a variety of molecular interactions including molecular rearrangements, excited state reactions, energy transfer, photoinduced electron transfer, ground state complex formation and collision quenching.[23] Therefore, to evaluate the interaction of the metal complexes **1** and **2** with BSA, the absorption and emission profiles of BSA were recorded in the presence of increasing concentrations of each complex at 297 K in PBS (pH 7.4). The concentration of BSA was maintained at 10 μM and the concentration of the Re(I) complexes was varied between 0–10 μM. The absorbance spectrum of BSA exhibits a characteristic maxima at 280 nm, which can be attributed to the aromatic amino acids.[24-26] Upon incremental addition of either **1** or **2**, the absorbance was observed to increase linearly (UV-Visible absorption spectra of BSA in the presence of **1** or **2** are shown in Figure S1).

BSA exhibits a strong fluorescence emission at 346 nm when excited at 280 nm, with no emission recorded above 450 nm (Figure 2). In contrast, complexes **1** and **2** do not show

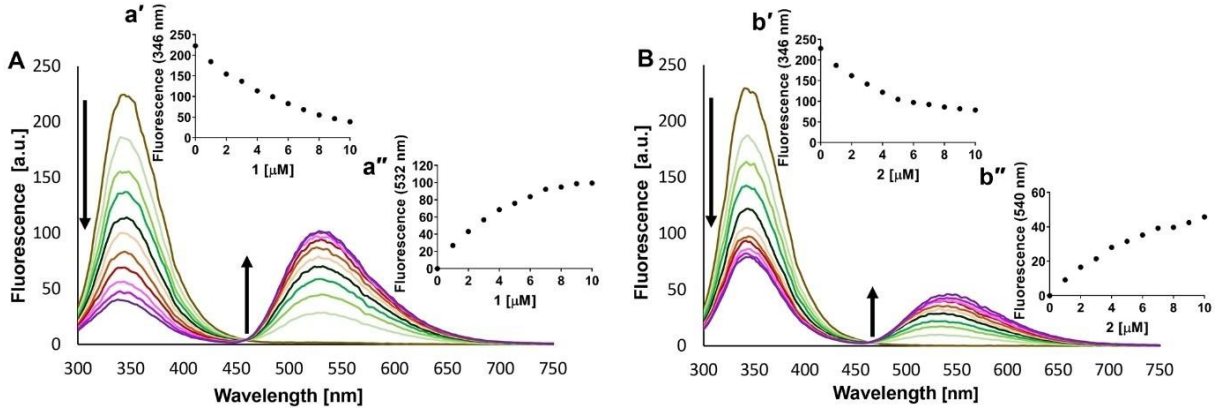

Figure 2. Fluorescence spectra changes observed upon increasing concentration (0–10 μM) of (A) complex **1** and (B) **2** at 280 nm excitation. The concentration of BSA was kept constant at 10 μM. Insets a' and b' show changes in fluorescence intensity at 346 nm as a function of the probe concentration, while insets a'' and b'' show changes in fluorescence intensity at 530–540 nm, respectively, as a function of the probe concentration.

any emission below 450 nm (the emission from both complexes is detected between 480–720 nm) when excited at 280 nm, which is in accordance with Werrett et al.[19] Therefore, any changes in the band at 346 nm can be attributed to changes in the structure of BSA and not a contamination of signal from complexes **1** or **2**. Because Re(I) compounds show absorption at ~ 280 and ~ 346 nm (Figure S2), the fluorescence intensity results were corrected for the inner filter effect, as described in the Experimental Section. Upon increasing concentration of **1** or **2**, the fluorescence emission at 346 nm is quenched by approximately 82 % and 65 %, respectively (Figure 2). The observed quenching of BSA fluorescence suggests an interaction between the complexes and BSA, which may be of dynamic and/or static nature. Quenching continues until approximately 8 μM of **1** and 7 μM of **2** have been added, after which the fluorescence quenching of BSA emission begins to plateau. This is more noticeable for the titration of **2** to BSA (Figure 2B inset b'). No shift in emission maxima was observed in either titration.

Both Re(I) complexes are weakly emissive in PBS when excited at 280 nm (Figure S3), with an emission maximum observed at 552 nm. Interestingly, the emission maxima of complexes **1** and **2** is blue shifted to approximately 530 nm in the presence of BSA (Figure 2 and Figure S2 for the emission profile in the presence or absence of BSA, respectively). The shift suggests a change in environment for both complexes upon binding to BSA. Since the phosphorescent emission from both Re(I) complexes originates from excited states of charge transfer nature (as an admixture of metal-to-ligand and ligand-to-ligand charge transfer states-^{3}MLCT/^{3}LLCT), the band is sensitive to the polarity and rigidity of the local environment. As expected, increasing the concentration of either complex results in an increased emission at around 530 nm, which also forms a plateau at a similar point as was observed for the quenching of BSA. Interestingly, the emission from complex **2** is slightly red shifted by about 10 nm as the concentration of **2** increases in the solution (Figure 2B, inset b''), which is not observed for complex **1**; suggesting that there may be some differences in the binding interaction of **1** and **2** with BSA. The ratio of maximum fluorescence intensity (F_{max}) of Re(I) compounds at 530 nm (**1**) or 540 nm (**2**) to maximum BSA fluorescence intensity at 346 nm (F_{530}/F_{346} or F_{540}/F_{346}) plotted against Re(I) concentration gives a straight line (Figure S4), suggesting a ratiometric response. Thus, changes in F_{max} of Re(I) complexes are indicative of BSA F_{max} changes upon increasing concentration of either Re(I) compound.

To explore the effect of different excitation wavelengths, the emission profiles of complexes **1** and **2** was recorded upon excitation to the charge transfer manifold at 350 nm, as opposed to excitation to ligand centred π-π* excited states upon excitation at 280 nm. No plateau of emission at 530 nm was observed upon excitation at 350 nm. The emission intensity was observed to increase for both complexes (Figure S5), in contrast to excitation at 280 nm (Figure 2). This difference can be explained by the fact that excitation at 280 nm occurs predominantly at the BSA, followed by energy transfer to the interacting Re(I) complexes. On the other hand, excitation at 350 nm is absorbed directly by all the Re(I) complexes, whether they are free or in interaction with BSA.

The effect of adding variable amounts of BSA to Re(I) complexes on absorption and emission spectra

The next step to better understand the interaction between the Re(I) complexes and BSA was to titrate BSA (0–21 μM) into a fixed concentration of complexes **1** or **2** (3 μM) and monitor the effects on both the absorbance (Figure S6) and emission profiles, following both excitation at 280 nm and 350 nm (Figure 3). As expected, increasing the concentration of BSA resulted in enhanced emission intensity at 346 nm (Figure 3Aa' and Bb'). The emission increases linearly as a function of BSA concentration until about 18 μM, where it reaches a plateau that may be attributed to a self-quenching phenomenon.[27,28] Interestingly, the emission from both the Re(I) complexes initially increases as the concentration of BSA increased (up to 6 μM), from which point it then decreases linearly (Figure 3Aa'' and Bb''). Both complexes behaved in a similar manner when the shorter 280 nm excitation wavelength was used. When the longer wavelength excitation of 350 nm was used, the emission from each of the complexes was somewhat different. For complex **1**, the emission increases when the concentration of BSA is increased (Figure 3Cc'), whereas emission of complex **2** decreases (Figure 3Dd'); above BSA concentration of ~6 μM the emission from both complexes reaches a plateau. The emission from both complexes is again blue shifted in the presence of BSA.

BSA quenching mechanism

The addition of either complex to BSA results in emission quenching, and therefore a reduction in the fluorescence quantum yield of the BSA fluorophores. Decreases in fluorescence quantum yields can be caused by a variety of molecular interactions (energy transfer, molecular rearrangement, ground state complex formation, collisional quenching).[29-31] These interactions are generally separated into two broad mechanisms. Dynamic quenching results from collisions between the excited fluorophore and the quencher, which must occur within the lifetime of the excited fluorophore. On the other hand, static quenching occurs when a non-fluorescent ground-state complex forms between the fluorophore and the quencher.[32,33] These two mechanisms can be discriminated by their different temperature dependence. In the case of a static process, the value of the quenching constant (K_{sv}) usually decreases together with increasing temperature, since the higher temperature destabilises the interaction. On the other hand, when dynamic quenching is involved, K_{sv} is likely to increase at higher temperatures because of increased diffusion rates.[23] To test which method is operating, we employed the Stern-Volmer Equation (Eq. (1)), after fluorescence measurements at different temperatures (297–320 K) were conducted:

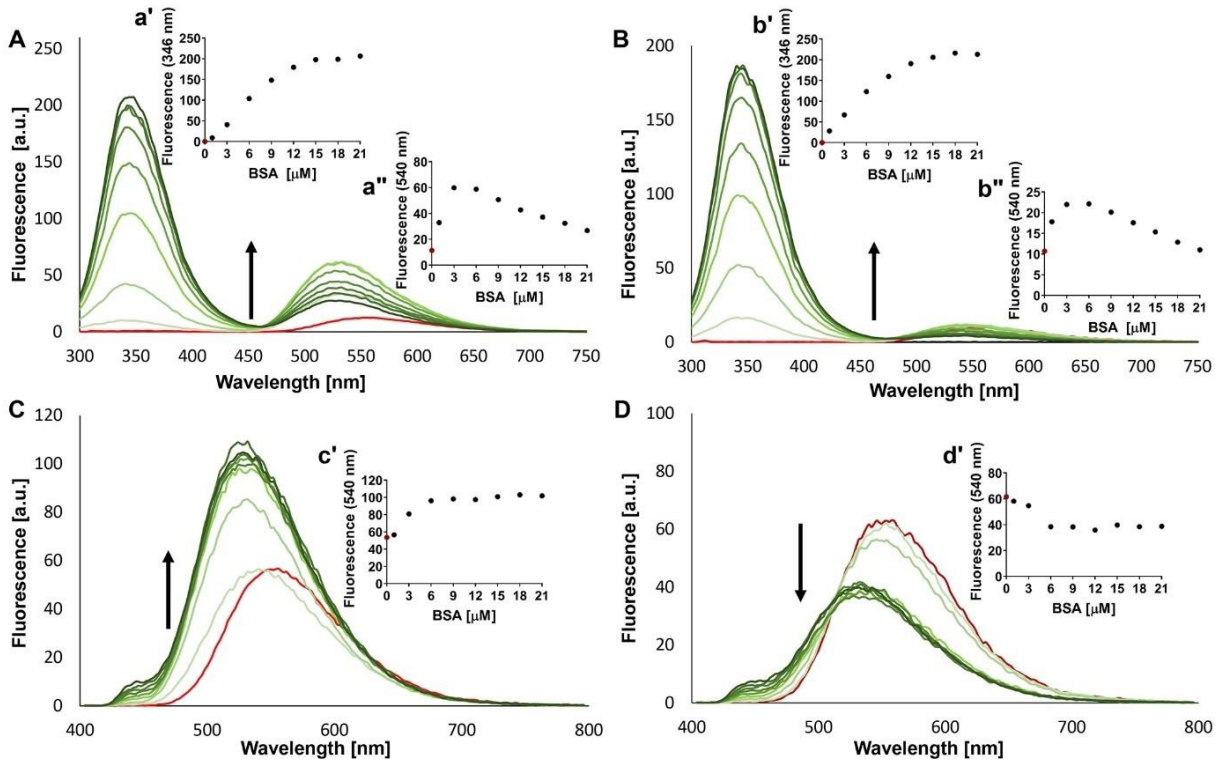

Figure 3. Fluorescence spectra changes observed upon increasing concentration of BSA (0-21 μM) added to complex (A, C) **1** and (B, D) **2** at (A, B) 280 nm and (C, D) 350 nm excitation. The given probe concentration was kept constant at 3 μM. Insets show changes in fluorescence intensity (Aa' and Bb') at 346 nm as a function of the BSA concentration and changes in fluorescence intensity (Aa'', Bb'', Cc' and Dd') at 540 nm as a function of BSA concentration.

$$\frac{F_0}{F} = 1 + K_{SV}[Q] \quad (1)$$

in which F_0 and F are relative fluorescence intensities in the absence and presence of the quencher, respectively, K_{sv} is the Stern-Volmer quenching constant, and [Q] is the concentration of quencher. $K_{sv} = k_q\tau_0$, in which k_q is the bimolecular quenching constant, τ_0 is the unquenched fluorescence lifetime, which for a biomacromolecule is assumed to be 10^{-8} s. Figure 4 shows Stern-Volmer plots for the complexes **1** (Figure 4A) and **2** (Figure 4C) at 297 K, 303 K, 310 K and 320 K. The plots reveal differences in Re(I) complex-protein interactions between **1** and **2**. In the case of **1**, the Stern-Volmer plot is linear until 6 μM of **1**. Then increasing the concentration of **1** results in a slight upward curvature. This type of non-linearity is generally observed when more than one quenching process occurs i. e. dynamic and static,[34-36] or there is more quenching at higher concentrations of the compound.[23,34,37,38] In order to calculate K_{sv} for **1** a modified Stern-Volmer Equation (2) was used:[35]

$$\frac{F_0}{F_0 - F} = \frac{1}{f_a K_{sv}[Q]} + \frac{1}{f_a} \quad (2)$$

where: f_a is the fraction of the initial fluorescence that is accessible to quencher and K_{sv} is the Stern-Volmer quenching

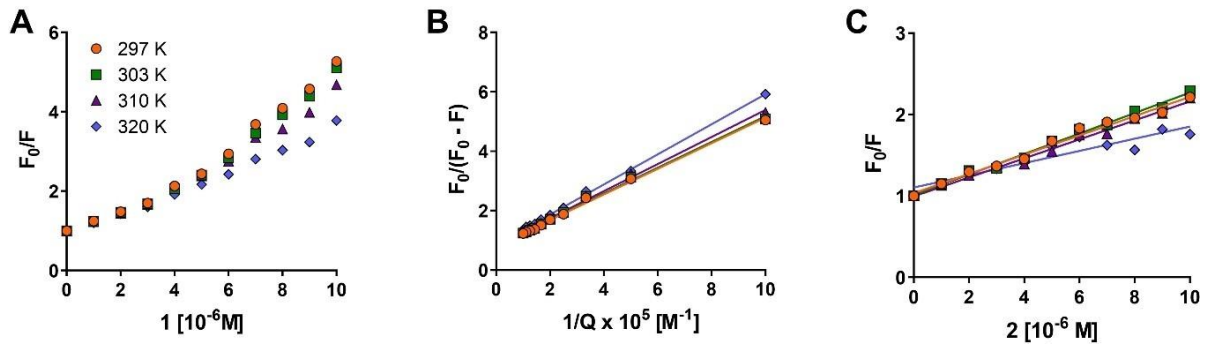

Figure 4. Stern-Volmer plots of BSA quenching by (A) complex **1**, (C) **2** and (B) a modified Stern-Volmer plot for complex **1**.

constant of the accessible fraction (the other terms remain the same as the previous Equation (1)). The modified Stern-Volmer plot (Figure 4B) shows linearity and the calculated K_{sv} decreases together with increasing temperature (Table 1), suggesting a static quenching mechanism. The Stern-Volmer plot for complex **2** (Figure 4C) shows a linear response between 297 K and 310 K, with no significant change in K_{sv}.

However, at 320 K the slope of the linear fitting decreases. The linear slope suggests that only one quenching mechanism is occurring, and the decrease in K_{sv} at higher temperatures suggests a static mechanism. The formation of a complex between BSA and **1** or **2** is confirmed by the values of the quenching rate constant k_q, which is calculated from Equation (3):[23]

$$k_q = \frac{Ksv}{t0} \quad (3)$$

in which τ_0 is the average lifetime of the fluorophore in the excited state (10^{-8} s). If a pure static quenching mechanism was occurring, then an increase in temperature would lead to a decrease in stability of the complex.[29,39] In contrast, for a dynamic effect, faster diffusion rates occur at higher temperature, which results in the increase in k_q.[40] Analysis of k_q for **2** shows that at temperatures between 297–310 K there is no difference in calculated k_q values. Above 310 K a decrease in k_q is observed which supports a static quenching (Figure 4B, Table 1). This data suggests that for both complexes a static quenching mechanism is mainly occurring. The K_{sv} values above 10^4 L mol^{-1} and k_q values above 2.0×10^{10} L mol^{-1} s^{-1} are indicative of strong interactions between **1** or **2** and BSA.[36,41,42] For complex **1** the upward trend from the initial Stern-Volmer plot may suggest that this complex is a very effective quencher for BSA, as there is limited evidence at this stage of dynamic quenching.

Determination of binding constant and binding sites

To calculate the binding constant (K_b) for BSA—Re(I) complexes and the number of binding sites (n), the following equation was employed:

$$Log\left[\frac{F_0 - F}{F}\right] = LogK_b + nLog[Q] \quad (4)$$

in which K_b is the binding constant and *n* is the number of binding sites (the other terms remain the same as for Equation (1)). A plot of log[(F_0—F)/F] *versus* log[*Q*] gives a straight line (Figure 5), where the slope equals n and the intercept on the y-axis equals log[K_b]. The calculated values of K_b and *n* are reported in Table 2. The *n* values for both **1** and **2** are approximately equal to 1, suggesting that BSA has one biding site for each Re(I) complex. To further support 1 : 1 binding, we also generated a plot based on Benesi-Hildebrand Equation (S1), the linearity of which indicates 1 : 1 complexation (Figure S7).[43] The strength of the binding can be deduced from the K_b, with higher values indicating stronger binding.[44] For a

Table 1. Stern-Volmer quenching constants and bimolecular quenching rate constants for the interaction of BSA with complex **1** and **2**.

T [K]	R^2		$K_{sv} \times 10^5$ [L mol^{-1}]		k_q 10^{13} [Lmol^{-1} s^{-1}]	
	1[a]	**2**	**1**[a]	**2**	**1**[a]	**2**
297	0.996	0.985	2.322	1.184	2.322	1.184
303	0.995	0.991	2.310	1.258	1.963	1.258
310	0.996	0.990	2.197	1.167	1.841	1.167
320	0.999	0.874	1.976	0.750	1.697	0.750

[a] Values for **1** were calculated using modified Stern-Volmer Equation (2).

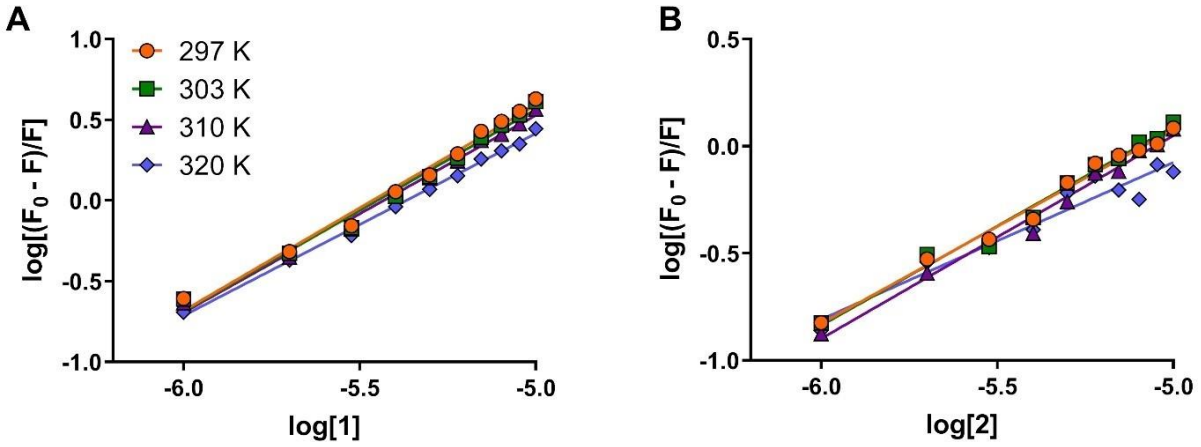

Figure 5. Double logarithmic plot employed to determine binding parameters for (A) complex **1** and (B) **2**.

Table 2. Binding parameters for the BSA-rhenium probes interaction.

T [K]	R^2		K_b [$Lmol^{-1}$]		n	
	1	**2**	**1** ($\times 10^6$)	**2** ($\times 10^4$)	**1**	**2**
297	0.987	0.988				
	9.09	4.06	1.27	0.91		
303	0. 986	0.983	6.76	5.43	1.25	0.93
310	0.991	0.987	4.36	6.19	1.22	0.95
320	0.997	0.935	1.15	0.39	1.13	0.73

potential use of compounds in life sciences, binding to the serum protein should be reversible, thus allowing transport of the compound as well as release at the target site. The ideal binding constant is considered to be in the range of 10^4-10^6 $L\,mol^{-1}$.[44] The K_b values for **1** and **2** are in this range and further indicate that **1** binds to BSA significantly stronger than **2** (the K_b value for **1** is two orders of magnitude higher than the value for **2**, Table 2). The different affinity for **1** and **2** versus BSA may result from interaction to different binding sites on BSA or a difference in the interaction with the same binding site caused by the nitrile and methyl ester substituents.

Generally, in the case of static quenching, the binding constant is expected to decrease together with increasing temperature due to destabilisation of the complex.[34,45] Such a decrease of K_b occurs for **1**, suggesting that a static quenching mechanism may be predominant between this Re(I) complex and the BSA protein. However, in the case of **2**, K_b increases together with temperature up to 310 K, and then decreases substantially at 320 K. This suggests that both dynamic and static mechanism may be operating. However, since the increase in temperature is known to strengthen hydrophobic interactions in aqueous solutions, it is possible that if the static quenching is caused by hydrophobic interactions then the binding constant may increase with temperature up to a certain point.[46,47] An increase in K_b values with temperature has been reported before, when static quenching mechanism was determined with different methods.[29,35]

Determination of thermodynamic parameters

Thermodynamic parameters, including enthalpy (ΔH), entropy (ΔS), and free energy (ΔG) of binding provide detailed information on interaction. To estimate these parameters, the van't Hoff Equation (5) and Equation (6) were employed:

$$Ln K_b = -\frac{\Delta H}{RT} + \frac{\Delta S}{R} \quad (5)$$

$$\Delta G = \Delta H - T\Delta S \quad (6)$$

where R is the gas constant. The negative values of both ΔH and ΔS indicate the contribution of van der Waals forces and hydrogen bonding, while the positive values of ΔH and ΔS demonstrate that hydrophobic interaction dominate. If ΔH is negative but ΔS is positive, electrostatic forces play the major role in binding.[41,48,49] The thermodynamic parameters were obtained from the van't Hoff plots (Figure 6). For compound **2** only the first three temperatures were used, where the increase in K_b values with the increasing temperature was observed. At 320 K, there was a sudden decrease in K_b (Table 2). The thermodynamic parameter for BSA—Re(I) complex **1** and **2** are presented in Table 3. Negative values of ΔG for both complexes indicates that binding between BSA and Re(I) compounds is a spontaneous process. For complex **1** both ΔH and ΔS have negative values, suggesting that Van der Waals forces and hydrogen bonding play the major role in the interaction. Conversely, compound **2** showed positive values of ΔH and ΔS, indicating hydrophobic interactions were the main contributor.

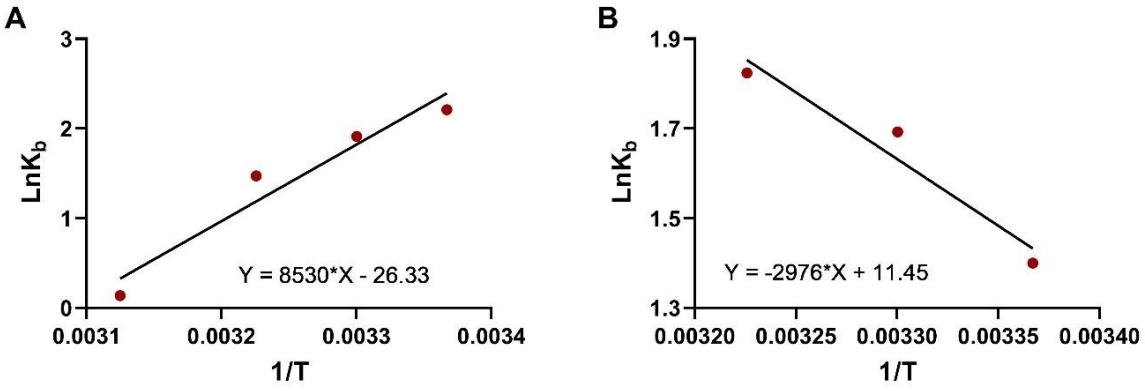

Figure 6. Van't Hoff plots for the binding interaction between BSA and **1** (A) and **2** (B).

Table 3. Thermodynamic parameters BSA—Re(I) complexes interaction.

T [K]	R^2		ΔH [kJmol^{-1}]		ΔS [J mol^{-1} K^{-1}]		ΔG [kJmol^{-1}]	
	1	**2**	**1**	**2**	**1**	**2**	**1**	**2**
297	0.937	0.939	−70	24	−218	95	−5.9	−3.5
303							−4.6	−4.1
310							−3.1	−4.8
320							−0.9	−5.7

This is in agreement with the idea described above, stating that if the static quenching is caused by hydrophobic interactions then the binding constant may increase with temperature up to a certain point.[46,47]

Energy transfer

The overlap between the emission spectrum of BSA (donor) and the absorption spectrum of complexes **1** and **2** (Figure 7), suggests that Förster resonance energy transfer (FRET) may take place as a mechanism for BSA quenching. For FRET to occur, the distance (r) between the donor and the acceptor has to be indicatively shorter than 8 nm.[41,50] The following equations were used to determine the FRET parameters:

$$E = 1 - \frac{F}{F_0} = \frac{R_0^6}{R_0^6 + r^6} \quad (7)$$

$$R_0^6 = (8.79 \times 10^{-25}) K^2 N^{-4} \Phi J \quad (8)$$

$$J = \frac{\int_{\lambda} F(\lambda)\varepsilon(\lambda)\lambda^4 d\lambda}{\int_{\lambda} F(\lambda) d\lambda} \quad (9)$$

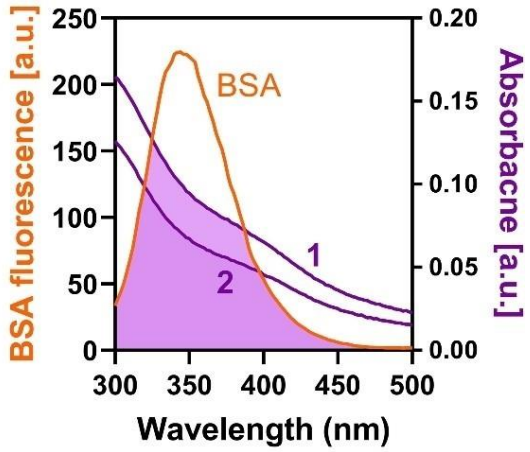

Figure 7. Spectral overlap between emission spectrum of BSA (excitation 280 nm) and absorption spectrum of Re(I) complexes **1** and **2**.

in which F_0 is the emission intensity of free BSA, F is the fluorescence intensity of BSA in the presence of the acceptor, E is energy transfer efficacy, R_0 is the Förster distance at which the energy transfer efficacy in 50 %, K^2 denotes a spatial orientation factor of donor and acceptor dipoles (here assumed to be 2/3), N represents the refractive index of the medium (1.336), Φ is the quantum yield of the donor (0.13) and J corresponds to the overlap integral between the emission spectrum of donor and the absorption spectrum of the acceptor. $F(\lambda)$ is the normalised fluorescence intensity of the donor at the wavelength λ, ε(λ) is the molar absorption coefficient of the acceptor at the wavelength λ.[23] The obtained FRET parameters are presented in Table 4 and show that the efficiency of energy transfer was higher for complex **1** than **2**. For both Re(I) complexes, the value of r was smaller than 8 nm and $0.5\ R_0 < r < 1.5\ R_0$, indicating that the energy transfer between BSA and Re(I) compounds occurs with high probability.[51] For complex **1**, the value of r was slightly smaller than for complex **2**, suggesting that **1** is spatially closer to emitting BSA domains.

Circular dichroism

In order to assess if the binding of **1** and **2** alters the secondary structure of BSA, circular dichroism (CD) measurements were performed. As shown in Figure S8, native α-helical BSA shows two negative absorption maxima at 208 and 223 nm, which is in accordance with previous reports.[29,52,53] The CD spectra of BSA in the presence of **1** (Figure S8A) or **2** (Figure S8B) remained unchanged, suggesting that the interaction between BSA and the Re(I) complexes does not significantly alter the secondary structure of the protein.

Competitive binding

BSA has two main hydrophobic binding sites, site I located in the subdomain IIA and site II located in the subdomain IIIA of the protein.[15,54] To determine the binding sites for the complexes, a displacement assay was performed using two well-known site markers, ibuprofen and warfarin. Ibuprofen is

Table 4. FRET parameters for BSA and Re(I) complexes at 297 K.

Donor	Acceptor	J 10^{14} [nm^{3}Lmol^{-1}cm^{-1}]	R_0 [nm]	E	r [nm]
BSA	Complex **1**	1.357	2.68	0.830	2.06
BSA	Complex **2**	1.041	2.57	0.636	2.34

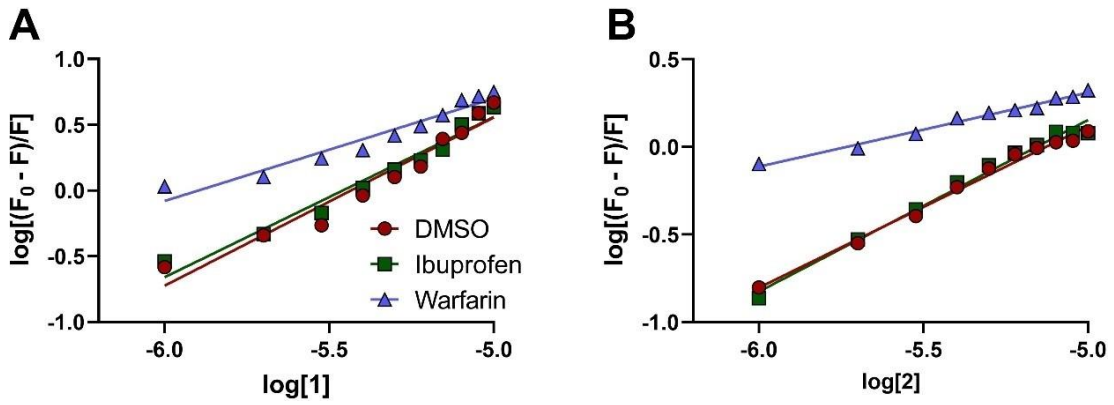

Figure 8. Double logarithmic plot employed to determine binding constants for (A) complex **1** and (B) **2** in the absence (DMSO) and presence of site markers, ibuprofen and warfarin.

known to bind to site II, while warfarin has high affinity for site I.[54-56] Figure 8 shows a plot of log[(F_0-F)/F)] versus log[Q] for complexes **1** (A) and **2** (B) in the absence and presence of site markers. The calculated binding constants are presented in Table 5. The binding constants decreased substantially for both rhenium complexes in the presence of warfarin, suggesting that **1** and **2** bind to a hydrophobic pocket in site I. In contrast, in the presence of ibuprofen, the binding constant of complex **1** was not significantly altered, suggesting that ibuprofen and **1** do not compete for the same binding site. For complex **2**, the binding constant increased when ibuprofen was added to the system. Such an increase has been reported before and can be explained by conformational changes in the protein structure caused by non-competitive binding of two different ligands.[57,58]

Molecular modelling

To further explain the binding mechanism between BSA and the Re(I) complexes, molecular modelling studies were performed using induced-fit docking (IFD), both following the standard protocol and using a custom protocol incorporating quantum-polarised ligand docking (QPLD). In the standard protocol, Glide Standard Precision docking and scoring is used, and the final docking score (referred to as IFDScore) is calculated as the sum of the obtained GlideScore from the final docking and 5 % of the determined Prime Energy following refinement of the initially docked complex. In the custom protocol, QPLD (as described in the Methods) is used in place of Glide Standard Precision docking and scoring, and the final docking score (here referred to as QPIFDScore) is calculated as the sum of the obtained score from the final QPLD docking and 5 % of the determined Prime Energy following refinement of the initially docked complex.

IFD was initially investigated for its ability to reproduce binding of 3,5-diiodosalicylic acid, naproxen and ketoprofen when docked to the unbound BSA structure, as well as to correctly rank the sites at which these molecules are observed to bind in the corresponding BSA-ligand complexes. Binding to three sites was investigated (Figure 9A); a site centred around Trp134, the ketoprofen-binding site (located on one side of Trp213; Site Ia), and the naproxen-binding site (located on the other side of Trp213; Site Ib). In all cases, the procedure was able to produce ligand poses close to their crystallographic placement, although performing better for 3,5-diiodosalicylic acid and naproxen, which feature rigid cores (Figure 9B—G), compared to the more flexible core of ketoprofen (Table 6). IFDScore was able to identify the correct binding site for all ligands, thus validating its use for predicting ligand binding modes and ligand binding sites on BSA. Redocking these poses using QPLD did not substantially change their conformation, and QPIFDScore yielded identical results for binding site assignment. However, QPIFDScore selects an alternative pose for ketoprofen with improved fit to the crystal structure (Figure 9D, E). In initial attempts to dock the rhenium compounds using IFD, partial charges derived by Jaguar were used; however, this resulted in the failure of compound **2** to dock to all sites (data not shown).

Using the default OPLS3e-derived charges for IFD yielded poses for both ligands at all sites, all of which were subsequently redocked successfully using QPLD. As poses of compound **2** passing the contact-based filter were not found at Site Ia and the site centred at Trp134, Site Ib (naproxen-binding site) is implicated as the preferred binding site for both compounds (Table 7), with compound **1** (Figure 10A) penetrating deeper into the site than compound **2** (Figure 10B). This is in agreement with K_b values being significantly higher for complex **2** than **1**.

Table 5. Binding constants of BSA-rhenium complexes in absence (DMSO) and presence of site markers, ibuprofen and warfarin.

Complex	*Kb* [$lmol^{-1}$] **1** ($\times 10^6$)	**2** ($\times 10^4$)
BSA+ DMSO	5.456	5.321
BSA+ ibuprofen	4.498	10.617
BSA+ warfarin	0.040	0.026

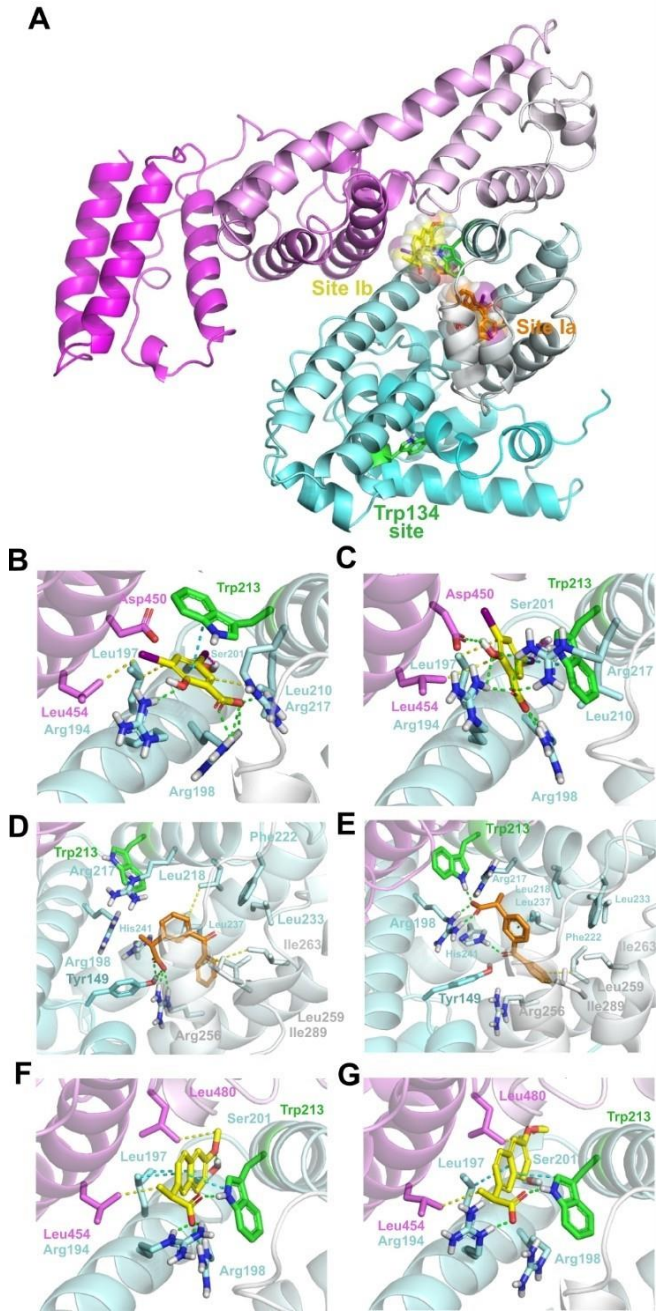

Figure 9. Validation of induced-fit docking for predicting ligand binding to BSA. (A) BSA structure indicating the three sites at which docking calculations were centred. (B) 3,5-diiodosalicylate bound to Site Ib. (C) 3,5-diiodosalicylate best pose following induced-fit docking (IFD) and quantum-polarised ligand docking (QPLD). (D) Ketoprofen bound to Site Ia. (E) Ketoprofen best pose following IFD and QPLD. (F) Naproxen bound to Site Ib. (G) Naproxen best pose following IFD and QPLD. Legend for all panels: BSA-cyan to magenta N-to-C terminus gradient; tryptophan-green; ligands binding to Site Ia-orange; ligands binding to Site Ib-yellow; hydrogen bonds-green dashes; nonpolar interactions-yellow dashes; π-π/CH-π interactions-cyan dashes; halogen bonds-magenta dashes.

BSA crystal structures show that ketoprofen (PDB 6QS9)[59] and warfarin (PDB 1H9Z and 1HA2)[60] bind to the same site in BSA subdomain IIA (Site Ia). Competitive binding assays showed that both Re(I) complexes displaced warfarin from its binding site (Site Ia), while molecular modelling suggests that both rhenium compounds bind to Site Ib. Site Ia and Ib are both located in subchambers of Sudlow Site I on the opposite sides of tryptophan residue. Thus, given the proximity of Site Ia and Ib, the observed competitive binding effect with warfarin likely results from the fact that molecules as large as Re(I) complexes, upon binding to Site Ib block entry to deeper located Site Ia. Indeed, it has been shown before that naproxen can displace warfarin from its binding site.[61,62] Overall, our data indicate that Re(I) complexes preferentially bind to Site Ib of BSA.

The tetrazole group of compound **1** forms a series of hydrogen bonds with the backbone of Val342 and Ser343, as well as a hydrogen bond with Arg217. Nonpolar interactions of note occur between the benzonitrile group with Leu197, Val342 and Leu480. The benzonitrile group also forms a CH-π interaction with Trp213. The majority of these interactions are reproduced by compound **2**, with the exception of the hydrogen bond to the Ser343 backbone, and the nonpolar interaction with Leu480. Other notable differences include the amine hydrogen of Trp213 forming a CH-π interaction with the compound's benzene ring, Val342 forming a CH-π interaction with the compound's tetrazole group, nonpolar interactions between the ester group and Leu197, and a π-π interaction between Arg217 and the phenanthroline ligand.

We demonstrated that IFD is capable of correctly identifying the binding sites and binding poses for drug-like molecules binding to BSA. By incorporating QPLD, improvements in the placement of more flexible molecules can be achieved, as well as a better description of partial charges in the rhenium compounds. Interestingly, incorporating quantum mechanically derived charges for the rhenium compounds in IFD results in failure of the compounds to dock to all sites, most likely as a result of IFD being optimised to use OPLS-derived charges. The developed protocol is similar to a previous utilised protocol for investigating binding of rhenium(I) complexes to fibrillar β-amyloid,[63] although without the added (and considerable) computational expense of molecular dynamics simulations; the validation of developed protocol performed (Table 6) demonstrates the sufficiency of the protocol for achieving meaningful results.

Conclusions

Photophysical studies support that the complexes **1** and **2** display strong affinity for BSA. This interaction does not cause a change in the secondary structure of BSA. Both **1** and **2** cause quenching of BSA fluorescent emission, and the corresponding Stern-Volmer plots and binding constants support a static mechanism. Interestingly, **1** and **2** showed different responses to increasing temperatures. Thermodynamic parameters suggest that different types of bonding interactions occur between BSA and the Re(I) complexes. Van der Waals forces and hydrogen bonding dominate for complex **1**, while hydrophobic forces play a major role for complex **2**. FRET analysis showed that energy transfer takes place between BSA and Re(I) compounds and that transfer efficiency is higher for complex **1**.

Table 6. Validation of induced-fit docking for predicting ligand binding to BSA.

Observed site[a]		3,5-diiodosalicylic acid Ia and Ib	Ketoprofen Ia	Naproxen Ib
IFDScore[b]	Site Ia	−827.80	−845.88	−840.86
	Site Ib	−832.84	−841.87	−850.17
	Trp134 site	−831.41	−833.57	−834.28
	Predicted site[c]	Ib	Ia	Ib
	RMSD[d]	2.0	4.4	1.2
QPIFDScore[b]	Site Ia	−827.59	−846.17	−841.46
	Site Ib	−832.62	−842.05	−850.74
	Trp134 site	−831.29	−834.13	−834.30
	Predicted site[c]	Ib	Ia	Ib
	RMSD[d]	2.0	3.3	1.2

[a] Determined from BSA-ligand crystal structure complexes. [b] Reported in kcal/mol. [c] Selected according to best IFDScore/QPIFDScore for any ligand pose at any site. [d] Root-mean-squared deviation reported only for pose with the best IFDScore/QPIFDScore at any site. Only calculated between ligand atoms. Reported in angstroms (Å).

Table 7. Induced-fit docking results for predicting rhenium complex binding to BSA.

		1	**2**
IFDScore[a]	Site Ia	−854.75	N/A[c]
	Site Ib	−859.37	−829.42
	Trp134 site	−838.91	N/A[c]
	Predicted site[b]	Ib	Ib
QPIFDScore[a]	Site Ia	−854.39	N/A[c]
	Site Ib	−858.85	−829.36
	Trp134 site	−838.71	N/A[c]
	Predicted site[b]	Ib	Ib

[a] Reported in kcal/mol. [b] Selected according to best IFDScore/QPIFDScore for any ligand pose at any site. [c] No poses passing Trp contact filter observed at this site.

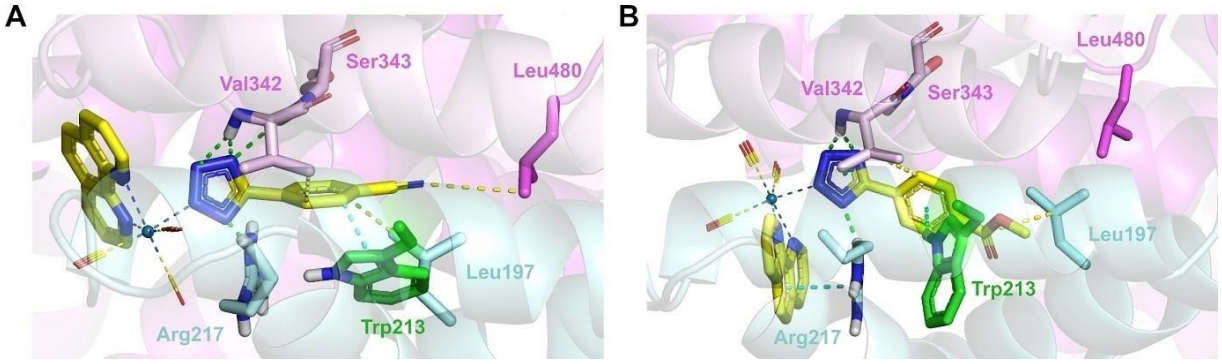

Figure 10. Prediction of rhenium complex binding to BSA. A) compound **1**. B) compound **2**. Legend for all panels: BSA-cyan to magenta N-to-C terminus gradient; tryptophan-green; ligand carbons-yellow; hydrogen bonds-green dashes; nonpolar interactions-yellow dashes; π-π/CH-π interactions-cyan dashes; metal-ligand bonds-teal dashes.

IFD and QPLD, performed together with competitive binding assay revealed that both Re(I) complexes likely bind to subdomain IIA (site I) of BSA and that the interaction is stronger for complex **1** than **2**. Our study showed that subtle functional group alterations modify binding properties of Re(I) complexes to the key serum protein, albumin, and this is anticipated to have an impact on future design of molecules for in vitro imaging and in vivo medical applications.

Experimental Section

Materials

All chemicals were of analytical reagent grade. All aqueous solutions were prepared using miliQ water. The complexes **1** and **2** were synthesised according to previously reported procedures.[19,20] Bovine serum albumin (BSA) (A7030) and phosphate buffered saline (PBS) (D108) were purchased from Sigma Aldrich.

Instrumentation

The absorption spectra were recorded using Varian Cary® 50 UV-Vis Spectrophotometer with a scan rate of 4800 nm/min. The emission spectra were obtained using Cary Eclipse Fluorescence Spectrophotometer with a scan rate of 1200 nm/min. The excitation and emission slits were kept at 5 nm. To record spectra at 297 K, 303 K, 310 K, and 320 K, the temperature in spectrophotometer was kept stable using a circulating water bath. Circular dichroism (CD) spectra were recorded using Jasco *J-815* spectropolarimeter.

Sample preparation

10 mM stock solutions of Re(I) complexes were prepared in DMSO (Sigma, D2650) and a 1 mM BSA stock solution was prepared in PBS. Stock solutions of both BSA and Re(I) complex were diluted in PBS to obtain desired working concentrations.

Absorption/emission studies-increasing concentration of the probes

BSA concentration was kept constant at 10 μM, while the concentration of Re(I) complexes increased from 0–10 μM. The emission spectra were recorded using two excitation wavelengths: 280 nm and 350 nm. The experiments were repeated two to three times with similar results. Since Re(I) compounds exhibit absorbance at ~ 280 and ~ 346 nm (excitation and emission of BSA, respectively), the fluorescence intensities were corrected for the inner filter effect using the following equation:

$$F_{corr} = F_{obs}\, 10^{(Alex+Alem)/2} \quad (10)$$

where, F_{corr} and F_{obs} are the corrected and the observed emission intensities, respectively, while $A\lambda_{ex}$ and A_{em} represent the absorbance at the excitation and the emission wavelengths, respectively.

Absorption/emission studies-increasing concentration of BSA

The concentrations of Re(I) complexes were kept constant at 3 μM, while the concentration of BSA increased from 0–21 μM. The emission spectra were recorded using two excitation wavelengths: 280 nm and 350 nm. The experiments were repeated three times with similar results.

CD measurements

The CD spectra of BSA (3 μM) were recorded in the presence and absence of Re(I) complexes in the far UV-CD range of 200–260 nm. The measurements were performed at 297 K using a 1 mm path length cuvette. Spectra were collected with a scan speed of 50 nm/min. BSA to Re(I) complex ratios were kept the same as for absorption/emission studies.

Competitive binding assay

Warfarin and ibuprofen were used for the competitive binding assay as they are known to bind to site I in subdomain IIA and site II in subdomain IIIA, respectively. Different concentrations (0–10 μM) of Re(I)complexes **1** and **2** were added to an equimolar solution of BSA and the relative competitor (10 μM). Fluorescence spectra were recorded after excitation with 280 nm wavelength to determine binding constants. The experiments were repeated two times with similar results.

Molecular modelling

Molecular modelling was performed using indicated tools available within Schrodinger Suite 2018–3. The structures of unbound BSA (PDB 4F5S)[64] and its complexes with 3,5-diiodosalicylic acid (PDB 4JK4),[65] naproxen (PDB 4OR0)[62] and ketoprofen (PDB 6QS9)[59] were obtained from the Protein Data Bank and prepared using the Protein Preparation Wizard. Missing side-chains and loops were added using Prime,[66] all water molecules removed, bound ligands processed via Epik to assign the appropriate charge/tautomeric state at pH 7.0,[67] and protein side-chain charge/tautomer assignment at pH 7.0 performed by PROPKA.[68] 3,5-diiodosalicylic acid, naproxen and ketoprofen structures used for docking were extracted from the crystal structure complexes following the protein preparation procedure. Rhenium compounds were prepared for docking from the crystal structures by first assigning bond orders, formal charges and Macromodel atom types to the atoms in the complexes. As rhenium is not specifically parameterised for OPLS3e, it was treated as a generic six-coordinate octahedral atom (Macromodel atom type GM).

Induced-fit docking (IFD)[69] was performed to the unbound BSA at three sites (defined as detailed in the Supporting Information; Table S1) using the standard protocol and default settings, and poses scored according to IFDScore (calculated as the sum of the Glidescore and 5 % of the Prime Energy). Each pose was subsequently redocked into the induced protein conformation using quantum polarised ligand docking (QPLD); Jaguar[70] was used to calculate ligand partial charges at the Accurate level (6-31G*/LACVP* basis sets with B3LYP density functional and ultrafine SCF accuracy level), and one pose returned per docking run. An adjusted IFDScore incorporating the QPLD results, referred to as QPIFDScore, was calculated for each pose, wherein the Glidescore obtained from QPLD was added to 5 % of the Prime Energy obtained from IFD adjusted for the difference in ligand internal energy obtained between IFD and QPLD. Poses of rhenium compounds were additionally filtered to select only those where the phenyltetrazole ligand makes at least one contact to Trp134 or Trp213, given by an atom-atom distance of no greater than 3.9 Å.

Acknowledgements

Funding from an Envision Sciences Research Translation Grant was used to support the study.

Keywords: bovine serum albumin · fluorescence spectroscopy · molecular modelling · rhenium complexes · UV/Vis spectroscopy

[1] J. G. Vaughan, B. L. Reid, S. Ramchandani, P. J. Wright, S. Muzzioli, B. W. Skelton, P. Raiteri, D. H. Brown, S. Stagni, M. Massi, *Dalton Trans.* **2013**, *42*, 14100–14114.
[2] C. A. Bader, R. D. Brooks, Y. S. Ng, A. Sorvina, M. V. Werrett, P. J. Wright, A. G. Anwer, D. A. Brooks, S. Stagni, S. Muzzioli, M. Silberstein, B. W. Skelton, E. M. Goldys, S. E. Plush, T. Shandala, M. Massi, *RSC Adv.* **2014**, *4*, 16345–16351.
[3] C. A. Bader, A. Sorvina, P. V. Simpson, P. J. Wright, S. Stagni, S. E. Plush, M. Massi, D. A. Brooks, *FEBS Lett.* **2016**, *590*, 3051–3060.
[4] C. A. Bader, T. Shandala, E. A. Carter, A. Ivask, T. Guinan, S. M. Hickey, M. V. Werrett, P. J. Wright, P. V. Simpson, S. Stagni, N. H. Voelcker, P. A. Lay, M. Massi, S. E. Plush, D. A. Brooks, *PLoS One* **2016**, *11*, e0161557.
[5] K. K. W. Lo, *Acc. Chem. Res.* **2015**, *48*, 2985–2995.
[6] C. A. Bader, E. A. Carter, A. Safitri, P. V. Simpson, P. Wright, S. Stagni, M. Massi, P. A. Lay, D. A. Brooks, S. E. Plush, *Mol. BioSyst.* **2016**, *12*, 2064–2068.

[7] V. Fernández-Moreira, F. L. Thorp-Greenwood, M. P. Coogan, *Chem. Commun.* **2010**, *46*, 186–202.
[8] A. Carreñ, A. E. Aros, C. Otero, R. N. Polanco, M. Gacitú, R. Arratia-Pé Rez Ab, J. A. Fuentes, *New J. Chem.* **2140**, *41*, 2140–2147.
[9] K. Ranasinghe, S. Handunnetti, I. C. Perera, T. Perera, *Chem. Cent. J.* **2016**, *10*, 71.
[10] G. Makris, L. L. Radford, M. Kuchuk, F. Gallazzi, S. S. Jurisson, C. J. Smith, H. M. Hennkens, *Bioconjugate Chem.* **2018**, *29*, 4040-4049.
[11] M. T. Gabr, F. C. Pigge, *Chem. A Eur. J.* **2018**, *24*, 11729-11737.
[12] S. Imstepf, V. Pierroz, R. Rubbiani, M. Felber, T. Fox, G. Gasser, R. Alberto, *Angew. Chem. Int. Ed.* **2016**, *55*, 2792–2795; *Angew. Chem.* **2016**, *128*, 2842–2845.
[13] A. Sorvina, C. A. Bader, C. Caporale, E. A. Carter, I. R. D. Johnson, E. J. Parkinson-Lawrence, P. V. Simpson, P. J. Wright, S. Stagni, P. A. Lay, M. Massi, D. A. Brooks, S. E. Plush, *Oncotarget* **2018**, *9*, 35541–35552.
[14] T. Peters, *All About Albumin: Biochemistry, Genetics, and Medical Applications*, Elsevier, **1995**, 285–318.
[15] D. C. Carter, J. X. Ho, *Adv. Protein Chem.* **1994**, *45*, 153–176.
[16] P. Singh, H. Singh, V. Castro-Aceituno, S. Ahn, Y. J. Kim, D. C. Yang, *RSC Adv.* **2017**, *7*, 15397–15407.
[17] E. Ahmad, P. Sen, R. H. Khan, *Cell Biochem. Biophys.* **2011**, *61*, 313–325.
[18] B. X. Huang, H. Y. Kim, C. Dass, *J. Am. Soc. Mass Spectrom.* **2004**, *15*, 1237–1247.
[19] M. V. Werrett, D. Chartrand, J. D. Gale, G. S. Hanan, J. G. MacLellan, M. Massi, S. Muzzioli, P. Raiteri, B. W. Skelton, M. Silberstein, S. Stagni, *Inorg. Chem.* **2011**, *50*, 1229–1241.
[20] P. J. Wright, S. Muzzioli, M. V. Werrett, P. Raiteri, B. W. Skelton, D. S. Silvester, S. Stagni, M. Massi, *Organometallics* **2012**, *31*, 7566–7578.
[21] P. F. Spahr, J. T. Edsall, *J. Biol. Chem.* **1964**, *239*, 850-854.
[22] B. J. H. Kuipers, H. Gruppen, *J. Agric. Food Chem.* **2007**, *55*, 5445-5451.
[23] J. R. Lakowicz, *Principles of Fluorescence Spectroscopy*, Springer-Verlag, **2006**.
[24] H. Xu, N. Yao, H. Xu, T. Wang, G. Li, Z. Li, *Int. J. Mol. Sci.* **2013**, *14*, 14185-14203.
[25] P. Ju, H. Fan, T. Liu, L. Cui, S. Ai, *J. Lumin.* **2011**, *131*, 1724-1730.
[26] L. Zhao, R. Liu, X. Zhao, B. Yang, C. Gao, X. Hao, Y. Wu, *Sci. Total Environ.* **2009**, *407*, 5019-5023.
[27] R. F. M. De Almeida, L. M. S. Loura, M. Prieto, A. Watts, A. Fedorov, F. J. Barrantes, *Biophys. J.* **2004**, *86*, 2261–2272.
[28] M. Ghosh, S. Nath, A. Hajra, S. Sinha, *J. Lumin.* **2013**, *141*, 87-92.
[29] V. D. Suryawanshi, L. S. Walekar, A. H. Gore, P. V. Anbhule, G. B. Kolekar, *J. Pharm. Anal.* **2016**, *6*, 56-63.
[30] G. Paramaguru, A. Kathiravan, S. Selvaraj, P. Venuvanalingam, R. Renganathan, *J. Hazard. Mater.* **2010**, *175*, 985–991.
[31] Y. Zhang, Y. Zheng, W. Xiong, C. Peng, Y. Zhang, R. Duan, Y. Che, J. Zhao, *Sci. Rep.* **2016**, *6*, 27335.
[32] Y. Shi, H. Liu, M. Xu, Z. Li, G. Xie, L. Huang, Z. Zeng, *Spectrochim. Acta Part A* **2012**, *87*, 251–257.
[33] K. A. Paterson, J. Arlt, A. C. Jones, *Methods Appl. Fluoresc.* **2020**, *19*, 025002.
[34] B. K. Paul, D. Ray, N. Guchhait, *Phys. Chem. Chem. Phys.* **2013**, *15*, 1275-1287.
[35] N. Ghosh, R. Mondal, S. Mukherjee, *Langmuir* **2015**, *31*, 8074-8080.
[36] D. M. Togashi, A. G. Ryder, D. M. Mahon, P. Dunne, J. E. D. S. D. McManus, M. Fitzmaurice, *Diagnostic Opt. Spectrosc. Biomed. IV*, **2007**, *66281* K, DOI: 10.1117/12.728354.
[37] B. K. Paul, N. Ghosh, S. Mukherjee, *Langmuir* **2014**, *30*, 5921-5929.
[38] U. Anand, C. Jash, R. K. Boddepalli, A. Shrivastava, S. Mukherjee, *J. Phys. Chem. B* **2011**, *115*, 6312-6320.
[39] B. Qiu, L. Guo, M. Chen, Z. Lin, G. Chen, *Analyst* **2011**, *136*, 973-978.
[40] N. C. Bessas, L. A. Silva, M. Comar Júnior, R. G. Lima, *Luminescence* **2021**, 391–408.
[41] T. A. Wani, A. H. Bakheit, S. Zargar, M. A. Hamidaddin, I. A. Darwish, *PLoS One* **2017**, *12*, e0176015.
[42] M. P. Kesavan, G. G. V. Kumar, K. Anitha, L. Ravi, J. D. Raja, G. Rajagopal, J. Rajesh, *J. Photochem. Photobiol. B* **2017**, *173*, 499-507.
[43] M. Sasmal, R. Bhowmick, A. S. Musha Islam, S. Bhuiya, S. Das, M. Ali, *ACS Omega* **2018**, *3*, 6293–6304.
[44] T. Topală, A. Bodoki, L. Oprean, R. Oprean, *Clujul Med.* **2014**, *87*, 215-219.
[45] Y. He, P. Yin, H. Gong, J. Peng, S. Liu, X. Fan, S. Yan, *Sensors Actuators B. Chem.* **2011**, *157*, 8-13.
[46] J. A. Schellman, *Biophys. J.* **1997**, *73*, 2960-2964.
[47] E. van Dijk, A. Hoogeveen, S. Abeln, *PLoS Comput. Biol.* **2015**, *11*, 1004277.
[48] X. Peng, X. Wang, W. Qi, R. Huang, R. Su, Z. He, *Food Funct.* **2015**, *6*, 2712–2726.
[49] P. D. Ross, S. Subramanian, *Biochemistry* **1981**, *20*, 3096-3102.
[50] M. C. Chirio-Lebrun, M. Prats, *Biochem. Educ.* **1998**, *26*, 320-323.
[51] B. Valeur, M. N. Berberan-Santos, *Molecular Fluorescence: Principles and Applications, Second Edition*, Wiley-VCH Verlag GmbH, **2001**, p. 247–250.
[52] T. M. Goszczyński, K. Fink, K. Kowalski, Z. J. Leśnikowski, J. Boratyński, *Sci. Rep.* **2017**, *7*, 9800.
[53] A. T. Buddanavar, S. T. Nandibewoor, *J. Pharm. Anal.* **2017**, *7*, 148-155.
[54] G. Sudlow, D. J. Birkett, D. N. Wade, *Mol. Pharmacol.* **1976**, *12*, 1052-1061.
[55] Z. M. Li, C. W. Wei, Y. Zhang, D. S. Wang, Y. N. Liu, *J. Chromatogr. B* **2011**, *879*, 1934-1938.
[56] I. Sedov, A. Nikiforova, D. Khaibrakhmanova, *Int. J. Pharm.* **2020**, *583*, 119362.
[57] S. D. Stojanović, J. M. Nićiforović, S. M. Živanović, J. V. Odović, R. M. Jelić, *Monatshefte fur Chemie* **2020**, *151*, 999-1007.
[58] N. Seedher, P. Agarwal, *J. Lumin.* **2010**, *130*, 1841-1848.
[59] R. Castagna, S. Donini, P. Colnago, A. Serafini, E. Parisini, C. Bertarelli, *ACS Omega* **2019**, *4*, 13270-13278.
[60] I. Petitpas, A. A. Bhattacharya, S. Twine, M. East, S. Curry, *J. Biol. Chem.* **2001**, *276*, 22804-22809.
[61] N. M. Davies, K. E. Anderson, *Clin. Pharmacokinet.* **1997**, *32*, 268-293.
[62] A. Bujacz, K. Zielinski, B. Sekula, *Proteins Struct. Funct. Bioinf.* **2014**, *82*, 2199-2208.
[63] A. Aliyan, T. J. Paul, B. Jiang, C. Pennington, G. Sharma, R. Prabhakar, A. A. Martí, *Chem* **2017**, *3*, 898-912.
[64] A. Bujacz, *Acta Crystallogr. Sect. D* **2012**, *68*, 1278-89.
[65] B. Sekula, K. Zielinski, A. Bujacz, *Int. J. Biol. Macromol.* **2013**, *60*, 316-324.
[66] M. P. Jacobson, D. L. Pincus, C. S. Rapp, T. J. F. Day, B. Honig, D. E. Shaw, R. A. Friesner, *Proteins Struct. Funct. Genet.* **2004**, *55*, 351-67.
[67] J. C. Shelley, A. Cholleti, L. L. Frye, J. R. Greenwood, M. R. Timlin, M. Uchimaya, *J. Comput.-Aided Mol. Des.* **2007**, *21*, 681-91.
[68] M. H. M. Olsson, C. R. SØndergaard, M. Rostkowski, J. H. Jensen, *J. Chem. Theory Comput.* **2011**, *7*, 525-537.
[69] W. Sherman, T. Day, M. P. Jacobson, R. A. Friesner, R. Farid, *J. Med. Chem.* **2006**, *49*, 534-553.
[70] A. D. Bochevarov, E. Harder, T. F. Hughes, J. R. Greenwood, D. A. Braden, D. M. Philipp, D. Rinaldo, M. D. Halls, J. Zhang, R. A. Friesner, *Int. J. Quantum Chem.* **2013**, *113*, 2110-2142.

FULL PAPER

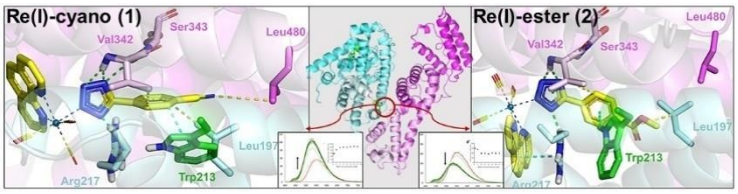

Interactions between bovine serum albumin (BSA) and two Re(I) complexes, differing in the functionality attached to the tetrazole, were investigated using spectroscopic methods and molecular modelling. Molecular docking was applied for the first time using Re(I) complexes as binding partners for BSA. This study revealed that subtle changes in the functional group of Re(I) complexes influence their interactions with BSA.

Dr. J. Lazniewska, Dr. M. Agostino, Dr. S. M. Hickey, Dr. E. Parkinson-Lawrence, Dr. S. Stagni, Dr. M. Massi, Dr. D. A. Brooks, Dr. S. E. Plush**

Spectroscopic and Molecular Docking Study of the Interaction between Neutral Re(I) Tetrazolate Complexes and Bovine Serum Albumin